A Grid-resolved Analysis of Base Flowfield for a Four-Engine Clustered Nozzle Configuration

Ten-See Wang
ED32, Computational Fluid Dynamics Branch
NASA Marshall Space Flight Center, Huntsville, Alabama 35812
(205)544-0503/FAX:(205)544-1215

AASRC Symposium Proceedings, Category: Heat Transfer, Combustion and Propulsion

Abstract

The objective of this study is to propose a computational methodology that can effectively anchor the base flowfield of a four-engine clustered nozzle configuration. This computational methodology is based on a three-dimensional, viscous flow, pressure-based computational fluid dynamics (CFD) formulation. For efficient CFD calculation, a Prandtl-Meyer solution treatment is applied to the algebraic grid lines for initial plume expansion resolution. As the solution evolves, the computational grid is adapted to the pertinent flow gradients. The CFD model employs an upwind scheme in which second- and fourth-order central differencing schemes with artificial dissipation are used. The computed quantitative base flow properties such as the radial base pressure distributions, model centerline static pressure, Mach number and impact pressure variations, and base pressure characteristic curve agreed reasonably well with those of the measurement.

Nomenclature

A_c area between nozzles in the exit plane

A_v vent area between nozzles

C_1 turbulence modeling constant

C_2 turbulence modeling constant

G geometrical matrices

h enthalpy

J	Jacobian of coordinate transformation
k	turbulent kinetic energy
M	Mach number
Pr	turbulent kinetic energy production
P	pressure
q	represents 1,u,v,w,h,k, and ε
S_q	source term for equation q
t	time
U	contravariant velocity
u^*	wall-friction velocity, = $(\tau_w/\rho)^{1/2}$
u^+	non-dimensional velocity, = u/u^*
u,v,w	mean velocities in x, y and z directions
x,y,z	physical coordinates
y^+	non-dimensional distance, = $y_p u^* \rho/\mu$
y_p	off-wall grid point distance to wall
α	conical nozzle half angle (=17.8°)
β	Prandtl-Meyer expansion angle
γ	specific heat
ε	turbulent kinetic energy dissipation rate
μ	effective viscosity
ξ	computational coordinates
ρ	density
σ_q	turbulence modeling constants
Φ	energy dissipation function

τ_w shear stress on the wall

θ initial plume expansion angle

ζ_i grid adaption weighing parameter

Subscripts

a ambient or test cell

b base

bc model centerline property on base

e nozzle exit

i impact probe property

o nozzle total property

w solid wall

Introduction

Excessive base heating has been a problem for many launch vehicles[1]. For certain designs such as the direct dump of turbine exhaust inside and at the lip of the nozzle[2], the potential burning of the turbine exhaust in the base region can be of great concern. Therefore, accurate prediction of the base environment at altitudes is very important during the vehicle design phase. Otherwise, the consequences could be undesirable. In the recent past, however, base environment of a launch vehicle has been predicted with large uncertainties using empirical methods, which either lead to out-of-database extrapolations, or overly conservative designs of the thermal protection system (TPS) and hence reduced payloads. The CFD method, which can be generically accurate when anchored, may provide a complementary prediction role, or be an optional design tool.

In a previous study[3], the turbulent base flowfield of a cold flow experimental investigation[4] for a four-engine clustered nozzle was numerically benchmarked. Parametric studies were performed on four

unadapted, relatively coarse algebraic grids (grid density varied from 34,030 to 113,202 points). Qualitative base flow features such as the reverse jet, wall jet, plume-to-plume recompression shock, and impingement have been captured. The physical nature of these flow features was in excellent agreement with that described in the experiment. Quantitative results such as the radial base pressure distribution, Mach number and static pressure variations along model centerline, were performed for a selected ambient-to-total-pressure ratio (P_a/P_o) of 39×10^{-4}. In addition, the base pressure characteristic curve was computed. These results agreed reasonably well with those of the measurement though relatively coarse grids were used. However, the trends of the model centerline Mach number and pressure distributions near the four-plume impingement point need to be improved, and the reversal of the base pressure characteristic curve was not captured. Furthermore, the predictions for the radial base pressure and model centerline properties need to be broadened to other P_a/P_o ratios, and in general the prediction for the base pressure characteristic curve needs to be improved.

Obviously, as pointed out in Ref. 3, the grid resolution played a dominating role in deciding the accuracy of the base flow solution. Higher grid density often resulted in better predictions. Also, when the grid lines that stemmed from the nozzle lip were specified at an angle corresponding to that of a Prandtl-Meyer solution at $P_a/P_o = 39 \times 10^{-4}$, better predictions were obtained for the radial base pressure and the model centerline flow properties. In this study, further grid resolution studies were performed to demonstrate that the Prandtl-Meyer solution treatment for the initial plume expansion at different altitudes was highly efficient. In addition, as the solution evolved, flow gradient grid adaption was demonstrated to have greatly enhanced the efficiency and quality of the solutions, especially at higher altitudes where the plumes expanded to greater sizes and created stronger interactions. Pertinent base flow features such as the radial base pressure distributions, model centerline Mach number and pressure variations, and base pressure characteristic curve were computed and compared with the experiment, on a broadened database. Special base flow features such as the vent area choking and base shock were surveyed with the improved

solution. Knowing limited computational resources always prohibits unlimited increase of grid density; the proposed computational methodology will provide efficient and accurate base flow solutions for future launch vehicle TPS designs.

Governing Equations

The basic equations employed in this study to describe the base flowfield for a four-engine clustered nozzle are the three-dimensional, general-coordinate transport equations. A generalized form of these equations written in curvilinear coordinates is given by

$$(1/J)(\partial \rho q/\partial t) = \partial[-\rho U_i q + \mu G_{ij}(\partial q/\partial \xi_j)]/\partial \xi_i + (1/J)S_q$$

where q represents 1, u, v, w, h, k, and ε, respectively. These are equations of continuity, x, y and z momentum, enthalpy, turbulent kinetic energy, and turbulent kinetic energy dissipation rate. The standard two-equation k-ε turbulence model[5] closure is used to describe the turbulent flow. Turbulence modeling constants σ_q and source terms S_q are given in Table 1. These turbulence modeling constants are widely used for nozzle flows[6,7].

The equation of state for an ideal gas is employed for the closure of the above system of equations. The characteristic of the governing equations changes from mixed parabolic-hyperbolic for subsonic flows, to mainly hyperbolic for supersonic flows.

To solve the system of nonlinear partial differential equations, the methodology uses finite difference approximations to establish a system of linearized algebraic equations. An upwind scheme was employed to approximate the convective terms of the momentum, energy and continuity equations; the scheme is based on second and fourth order central differencing with artificial dissipation. The dissipation terms are constructed such that a fourth-order central and fourth-order damping scheme is activated in smooth

regions, and a second-order central and second-order damping scheme is used near shock waves.

Viscous fluxes and source terms are discretized using second-order central difference approximation. A pressure-based predictor plus multi-corrector solution method is employed so that flow over a wide speed range can be analyzed. The basic idea of this pressure-based method is to perform corrections for the pressure and velocity fields by solving a pressure correction equation so that velocity/pressure coupling is enforced, based on the continuity constraint at the end of each iteration. Details of the present numerical methodology are given by ref. 6-7.

Table 1 σ_q and S_q of the transport equations

q	σ_q	S_q
1	1.00	0
u	1.00	$- p_x + \nabla[\mu(u_j)_x] - 2/3(\mu\nabla u_j)_x$
v	1.00	$- p_y + \nabla[\mu(u_j)_y] - 2/3(\mu\nabla u_j)_y$
w	1.00	$- p_z + \nabla[\mu(u_j)_z] - 2/3(\mu\nabla u_j)_z$
h	0.95	$Dp/Dt + \Phi$
k	0.89	$\rho(P_r - \varepsilon)$
ε	1.15	$\rho(\varepsilon/k)(C_1P_r-C_2\varepsilon)$

Baseline Grid Generation

A typical layout of an unadapted computational grid is shown in Fig. 1. Due to the symmetrical nature of the flowfield, only 1/8 of this layout is generated and used for the actual calculation. The

boundary that is perpendicular to the center of the base is termed "model centerline". The two sides of the pie-shaped grid, as shown in Fig. 1, are the symmetry planes. For illustrative purposes, the symmetry plane that lies between the nozzles is named the "plume impingement symmetry plane", since the plume impingement line and the recompression shock will be on or attached to this surface, whereas the other one is termed the "nozzle symmetry plane", since it passes through the centerline of the nozzle. The centerline in which the two symmetry planes intersected is called the "model centerline". Two grid zones were created. The first zone started at the base and included the nozzle and the plume region. The second zone (the outer shell) is comprised of the ambient air, and a portion of the expanded plume. The baseline unadapted grids were generated using GENIE grid generator[8]. The four nozzles, which are conical with a cylindrical external shell, are equally spaced on a circular base (heat shield)[4], as shown in Fig. 2. The area ratio of the nozzles is 3.11 and the nozzle exit diameters are 2.67 inches. The base is located 2.0 inches from the nozzle exit plane, giving a theoretical minimum vent area between nozzles of approximately 2.0 by 2.0 inches. The radial location of the theoretical minimum vent area, the four planes perpendicular to the base and between nozzles, is approximately 2.3334 inches from the centerline, which gives a vent area ratio (A_v/A_c) of approximately 0.96. This model is a larger scale model than the one used in Ref. 9.

Boundary Conditions

To start the calculation, an axisymmetric nozzle flow solution at the prescribed total pressure was carried out in a separate manner. A typical centerline exit Mach number for a total pressure of 60 psia was computed as 2.62. The converged flow solution was then mapped to a three-dimensional nozzle flowfield and the exit flow properties were specified as a fixed inlet boundary. The nozzle lip, nozzle outer wall and the base were specified as wall boundaries. The exit planes of zone 1 and zone 2, the outer surface (shell) of zone 2, and the inlet plane of zone 2 (flush with the base shield plane) were specified

as exit boundaries. In addition, a fixed (ambient) pressure was imposed on the inlet plane of zone 2, in order to obtain a unique solution for the corresponding altitude. Flow properties at the wall, symmetry plane, and exit boundary were extrapolated from those of the interior domain.

A no-slip condition was imposed on the wall boundary and a tangency condition was applied at the symmetry plane. A modified wall function approach is employed to provide near-wall resolution which is less sensitive to the near-wall grid spacing. This is achieved by incorporating a complete velocity profile[10]. That is,

$$u^+ = \ln [(y^+ + 11)^{4.02}/(y^+ - 7.37y^+ + 83.3)^{0.79}] + 5.63 \tan^{-1}(0.12y^+ - 0.441) - 3.81$$

This complete velocity profile provides a smooth transition between Logarithmic law-of-the-wall and linear viscous sublayer velocity distributions.

Prandtl-Meyer Solution Treatment for Initial Plume Angle Resolution

It has been shown[3] that the initial plume angle grid resolution is essential to the accurate prediction of base flow properties. In that study, the predicted base flow properties showed vast improvement even though a fixed initial plume angle (based on Prandtl-Meyer solution for $P_a/P_o = 39 \times 10^{-4}$) was used. The natural extension of that work would be to construct an initial plume angle resolved algebraic grid for each pressure ratio according to the isentropic Prandtl-Meyer plume expansion theory. As shown in Fig. 3, the initial plume expansion angle can be expressed as

$$\theta = \alpha + \Delta\beta$$

with

$$\beta = [(\gamma+1)/(\gamma-1)]^{1/2} \tan^{-1}[(\gamma-1)/(\gamma+1)\ (M^2-1)]^{1/2} - \tan^{-1}(M^2-1)^{1/2}$$

where β is the Prandtl-Meyer expansion angle[11] through which a supersonic stream is turned to expand from M = 1 to M > 1. β_e is based on the nozzle exit Mach number calculated from a simple one-dimensional calculation[12]. β_a is based on the ambient-to-total-pressure ratio, which is equivalent to having a M_a on the plume boundary.

Solution-Adaptive Grid Generation

A multi-zone, Self-Adaptive Grid Evolution (SAGE) code[13], is used to refine the initial plume angle resolved algebraic computational grid. Its method is based on grid-point redistribution through local error minimization. The procedure is analogous to applying tension and torsion spring forces proportional to the local flow gradient at every point and finding the equilibrium position of the resulting system of grid points. Since Mach number contour is closely associated with the plume boundary layer, whereas the pressure gradient follows the recompression shock, these two flowfield variables were used as pertinent grid adaption parameters. The adaptive function is a combination of both and can be expressed as

$$\zeta_M \, \partial M/\partial \xi + \zeta_p \, \partial P/\partial \xi = \zeta_M \, M_\xi + \zeta_p \, P_\xi$$

Fig. 4 shows slices of four typical computational grids. Each slice is a portion of the nozzle symmetry plane and is bounded by the nozzle centerline and the model centerline. Grid A is an algebraic grid treated with Prandtl-Meyer solution for the initial plume angle resolution. Grid B is the result of Grid A adapted solely to a pressure solution. The clustered grid lines clearly exhibit the plume-to-plume recompression shock, although the shock on the nozzle symmetry plane is not as strong as that in between two nozzles, or the "minimum vent area" plane. Grid C is the outcome of grid A adapted entirely to a Mach number solution. The packed grid lines follow the plume boundary and the initial plume expansion angle resolved algebraic grid lines that stem from the nozzle lip. Notice the adaption was applied several

grid lines above the nozzle lip so as to maintain the initial expansion resolution. Grid D is the adaption of Grid A where 50% Mach number gradient and 50% pressure gradient were used as the adaptive function. The grid line clustering follows both the plume boundary layer and the recompression shock.

The computations were performed on a NASA/MSFC CRAY-YMP. The computational time for a typical calculation was estimated as 1.0×10^{-4} CPU seconds per grid per step. Approximately 3000 to 4000 iterations were required for a 119,016 grid points solution to reach approximate convergence and an additional 2000 iterations were needed for a higher grid density (e.g., 168,399 grid points) solution to converge when the initial flowfields were started afresh. The storage requirement of the CFD model is 40 words per grid point.

Results and Discussion

Static Pressure, Mach Number, and Impact Pressure Variations along Model Centerline

Static pressure, Mach number, and impact pressure comparisons along model centerline, assess the accuracy of the model prediction for the strength of the reverse jet. The accuracy of the model prediction, however, depends on proper computational grid distributions. Fig. 5 shows a comparison of variations along model centerline for $P_a/P_o = 39 \times 10^{-4}$. The effects of the Prandtl-Meyer solution treatment for initial plume angle resolution and solution-adaptive gridding were obvious: the solution with the highest grid density (245,493 grid points) in which initial plume expansion was not resolved, although it employed twice the number of points in the initial plume boundary layer (in comparison to the 119,016 points setup) and had the grid refined according to the pressure gradient, produced the worst comparison; whereas the solutions using a 45.4-degree initial plume angle resolution, including one solution that ran without any grid adaption, computed significantly better agreements with less than half of the grid points. Among those three solutions, the one using pressure-solution gradient adaption produced best centerline property comparisons with those of the experiment. The one using Mach number-solution gradient adaption did

not compare as well. This is because the model centerline properties are enclosed by the recompression shock where the solution is best predicted by grid following pressure gradient. This example clearly demonstrates the validity and efficiency of the proposed computational methodology.

Fig. 6 show the comparisons of static pressure, Mach number and impact pressure variations along model centerline for three ambient-to-total-pressure ratios. In subsonic flow region, the impact pressure was reduced through

$$P_i = P\,(1 + (\gamma - 1)/2\ M^2)^{\gamma/(\gamma-1)}$$

In supersonic flow region, assuming the pitot tube[4] is immersed behind a shock wave, the Rayleigh pitot formula[11] was used.

$$P_i = P\,[(\gamma+1)M^2/2]^{\gamma/(\gamma-1)}\{(\gamma+1)/[2\gamma M^2-(\gamma-1)]\}^{1/(\gamma-1)}$$

Although extensive grid parametric studies have been performed, for the purpose of clarity, only selected comparisons were shown. It can be seen that different initial plume expansion angles were applied for different ambient-to-total-pressure ratios. At $P_a/P_o = 20\text{x}10^{-4}$, where maximum model centerline base pressure and peak Mach number were measured, 168,399 grid points were required for additional resolution. In general, The predictions agreed reasonably well with those of the experiment. The impact pressure decreases from the plume impingement point (approximately at Z = 4.5 inches) to the reverse jet recompression location due to radial flow. Downstream of the recompression it remains constant due to the prevailing subsonic flow. In general, the peak Mach number increases and the valley static pressure decreases as the pressure ratio (P_a/P_o) drops, and the position of the peak Mach number moves toward the base as does the valley of the static pressure. The strength of the reverse jet also increases as the pressure

drops. At $P_a/P_o = 20x10^{-4}$, a base shock is formed between 0.5 to 1.0 inches from the base center. Due to high viscous dissipation and in general a weak reverse jet (in comparison to under-expanded supersonic nozzle jet direct impingement on a perpendicular surface), the base shock is a smeared shock[4], as evidenced by the moderate increase of static pressure over a finite distance. Fig. 7 shows the computed iso-pressure surfaces at $P_a/P_o = 20x10^{-4}$. The computed plume-to-plume recompression shock (iso-value = 40 lb_f/ft^2) resembles closely that of a S-IV four engine stage exhaust plume Schlieren photograph[14]. The base shock (iso-value = 18 lb_f/ft^2) is situated above the heat shield, in between nozzles.

Radial Base Pressure Distribution

Radial base pressure data were taken at the base along the plume impingement symmetry plane, hence the comparisons benchmark the model for the predictions of the reverse jet at base center and the wall jet in the vent area. It can be seen from Fig. 8, the computed radial base pressures agreed reasonably well with those of the experiment. For all three ambient-to-total-pressure ratios, the reverse jets had formed and the peak pressures occurred at the base center, whereas the radial base pressure decreased as the distance from the center of heat shield increased. The radial base pressure eventually dropped to that of the cell pressure, which is physically correct.

Base Pressure Characteristic Curve

The center base pressure variation with ambient pressure (altitude) has become known as the characteristic curve[4]. Representing the location of the severest environment on the base, it is one of the important parameters in designing the thermal protection system for the launch vehicles. Fig. 9 shows a comparison between the measurements and the predictions. Matz and Goethert data[9] from which an identical A_v/A_e ratio of 0.96, albeit a mere 0.80 inches distance between the base and nozzle exit plane, were selected and plotted along with Brewer data[4] for background comparison. Both experiments were

conducted over the characteristic range of P_{bc}/P_a from near 1.0 to near 4.0, corresponding to altitudes ranging from 22,800 feet to 122,500 feet. At $P_a/P_o = 100x10^{-4}$ or $P_{bc}/P_a = 1$, the four exhaust plumes do not interact much with each other, except some aspiration exists. As altitude increases or as pressure ratio drops, the plumes start to interact more and the aspiration decreases; In the mean time, base pressure decreases whereas a reverse jet and subsequently the wall jets take shape. The predicted base pressure characteristic curve agreed very well with those of the experiment[4]. The condition of $P_{bc}/P_a = 2$ indicates a choking condition for the wall jet if the system was an enclosed isentropic convergent-divergent nozzle, which obviously does not apply since we are dealing with a complicated three-dimensional turning wall jet in a vent area where the open-top can only be closed by expanding sonic plumes. The fact that Mach number gradient adaption was applied mostly for $P_a/P_o > 26x10^{-4}$ whereas pressure gradient adaption was used at lower pressure ratios indicating that characteristic base pressure is dominated by plume boundary layer resolution when the plumes are further apart; as the plumes close, the recompression shock becomes more important, and better base pressure was resolved by applying P_ξ adaption. In fact, the plumes closed completely at approximately $P_a/P_o = 23x10^{-4}$ where the minimum base pressure occurs. After that enclosure, P_{bc} raises to its maximum at $P_a/P_o = 20x10^{-4}$ where the wall jet boundary layer grows and accelerates to sonic velocity in the vicinity of the vent area at $P_{bc}/P_a = 4$. P_{bc} then decreases as the ambient pressure continues to drop until the vent areas are completely choked. Further reduction in ambient pressure would not change the base pressure significantly after the total choking, as indicated by the leveling-off of the predicted P_{bc} from $P_a/P_o = 10x10^{-4}$ to $1x10^{-4}$, albeit the experiments[4,9] stopped at $P_a/P_o = 15x10^{-4}$ and $10x10^{-4}$, respectively, due to hardware limitations.

Fig. 10 shows the computed sonic surfaces at $P_a/P_o = 1x10^{-4}$. There is an approximate ellipsoid-shaped sonic surface in the middle of the domain, manifesting the acceleration of the reverse jet. The complex-shaped vent area sonic surface, not resembling the theoretical minimum vent area plane (Fig. 2), sealed all the flow path with the plume sonic surface and created the total choking.

Conclusion

A computational methodology has been developed to benchmark the base flowfield of a four-engine clustered nozzle configuration. It is based on: a three-dimensional, viscous flow, pressure-based CFD formulation, a Prandtl-Meyer solution treatment for the algebraic grid which is proved to be computationally efficient for the initial plume expansion resolution, and the computational grid which is subsequently refined according to pertinent base flow physics. The predicted physical flow features such as the reverse jet, wall jet, recompression shocks due to plume-plume and reverse jet-base impingement, plume enclosure, and vent area choking are in reasonable agreement with those described in the experiment. The predicted quantitative results such as the radial base flow distribution, static pressure, Mach number and impact pressure variations along model centerline, and the base pressure characteristic curve also agreed well with those of the measurement. This methodology not only provides insight into the multiple engine base flow physics, but also will be useful in the design and analysis of TPS for launch vehicles.

References

[1] Dahm, W.K., "Present Techniques and Problems in the Determination of the Base Heating Environment of Propelled Booster and Space Vehicles," Proceedings of the Fifth International Symposium on Space Technology and Science, Sept. 1963, pp. 377-388.

[2] Tucker, P.K., and Croteau-Gillespie, M., "Combustion Devices Technology Team: An Overview and Status of STME-Related Activities," AIAA Paper 92-3224, July 1992.

[3] Wang, T.-S., "Numerical Analysis of Base Flowfield at High Altitude for a Four-Engine Clustered Nozzle Configuration," AIAA Paper 93-1923, June 1993.

[4] Brewer, E.B., and C.E. Craven, "Experimental Investigation of Base Flow Field at High Altitude for a Four-Engine Clustered Nozzle Configuration," NASA TND-5164, 1969.

[5] Launder, B.E., and Spalding, D.B., "The Numerical Computation of Turbulent Flows," Computer Methods in Applied Mechanics and Engineering, Vol. 3, No. 2, 1974, pp.269-289.

[6] Wang, T.-S., "Numerical Study of the Transient Nozzle Flow Separation of Liquid Rocket Engines," Computational Fluid Dynamics J., Vol.1, No.3, Oct. 1992, pp. 305-314.

[7] Wang, T.-S. and Y.-S. Chen, "Unified Navier-Stokes Flowfield and Performance Analysis of Liquid Rocket Engines," Journal of Propulsion and Power, Vol. 9, No. 5, Sept.-Oct. 1993, pp.678-685.

[8] Soni, B.K., "GENIE: Generation of Computational Grids for Internal-External Flow Configurations," Numerical Grid Generation in Computational Fluid Dynamics, S. Sengupta, J. Hauser, P.R. Eiseman, J.F. Thompson (eds.), Pineridge Press, 1988.

[9] Matz, R., and B.H. Gothert: Fluid Dynamic Aspects of Space Flight, Vol.II, Experimental Investigation of Base Flow Characteristics of Four Nozzle-Clustered Rocket Model. Gorden and Breach, AGARD graph 87, 1966.

[10] Liakopouls, A., "Explicit Representations of the Complete Velocity Profile in a Turbulent Boundary Layer," AIAA Journal, Vol. 22, No. 6, Jan. 1984, pp. 844-846.

[11] Ames research staff, "Equations, Tables, and Charts for Compressible Flow," Report 1135, Ames Aeronautical Laboratory, 1935.

[12] Svehla, R.A., and McBride, B.J., "FORTRAN IV Computer Program for Calculation of Thermodynamic and Transport Properties of Complex Chemical Systems," NASA TN D-7056, 1973.

[13] Davies, C.B., and E. Venkatapathy, "The Multidimensional Self-Adaptive Grid Code: SAGE," NASA TM 103905, July, 1992.

[14] Sergeant, R.J., "Base Heating Scaling Criteria for a Four-Engine Rocket Cluster Operating at High Altitude," AIAA Paper 65-826, December, 1965.

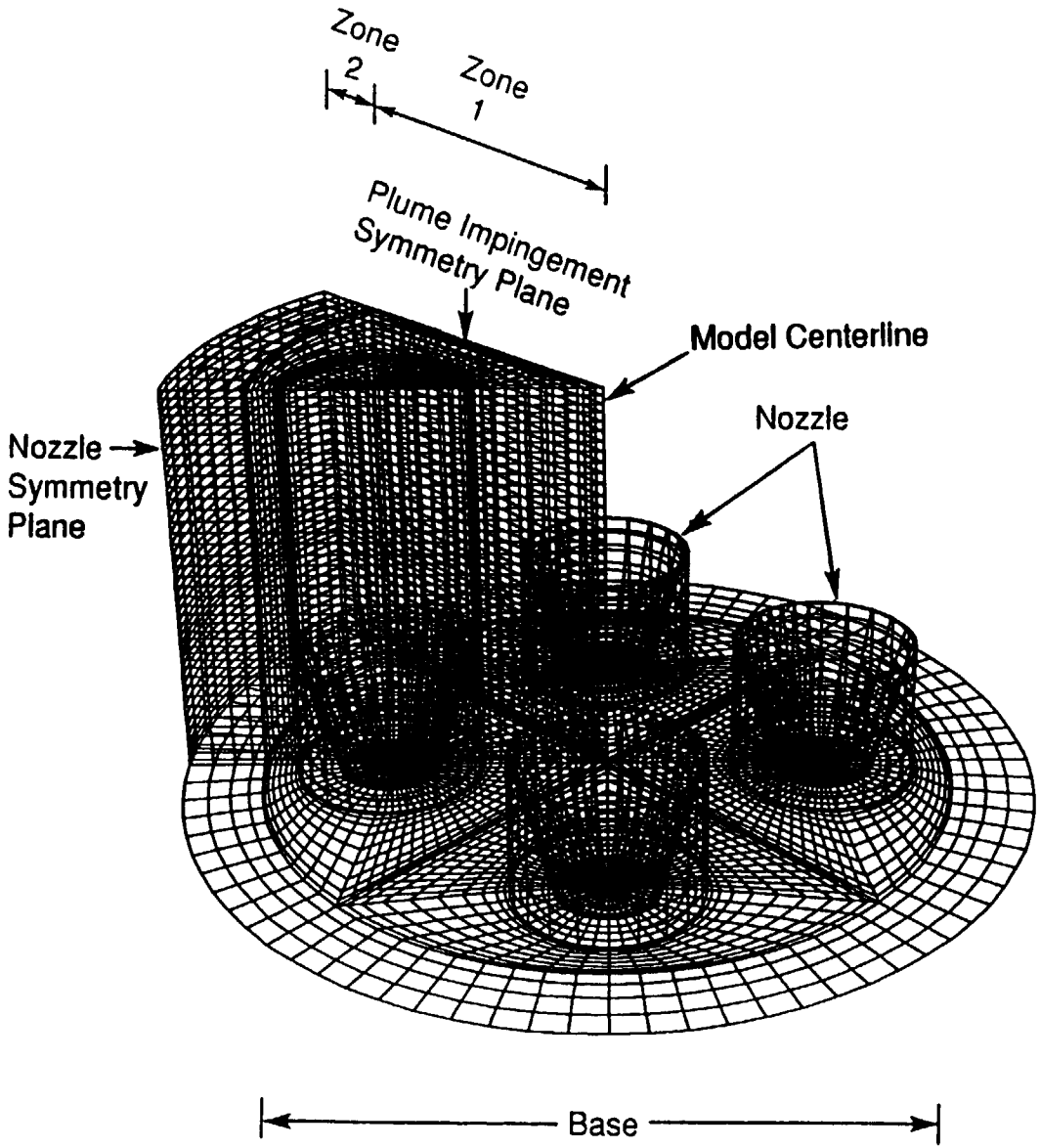

Fig. 1 Layout of a typical computational grid

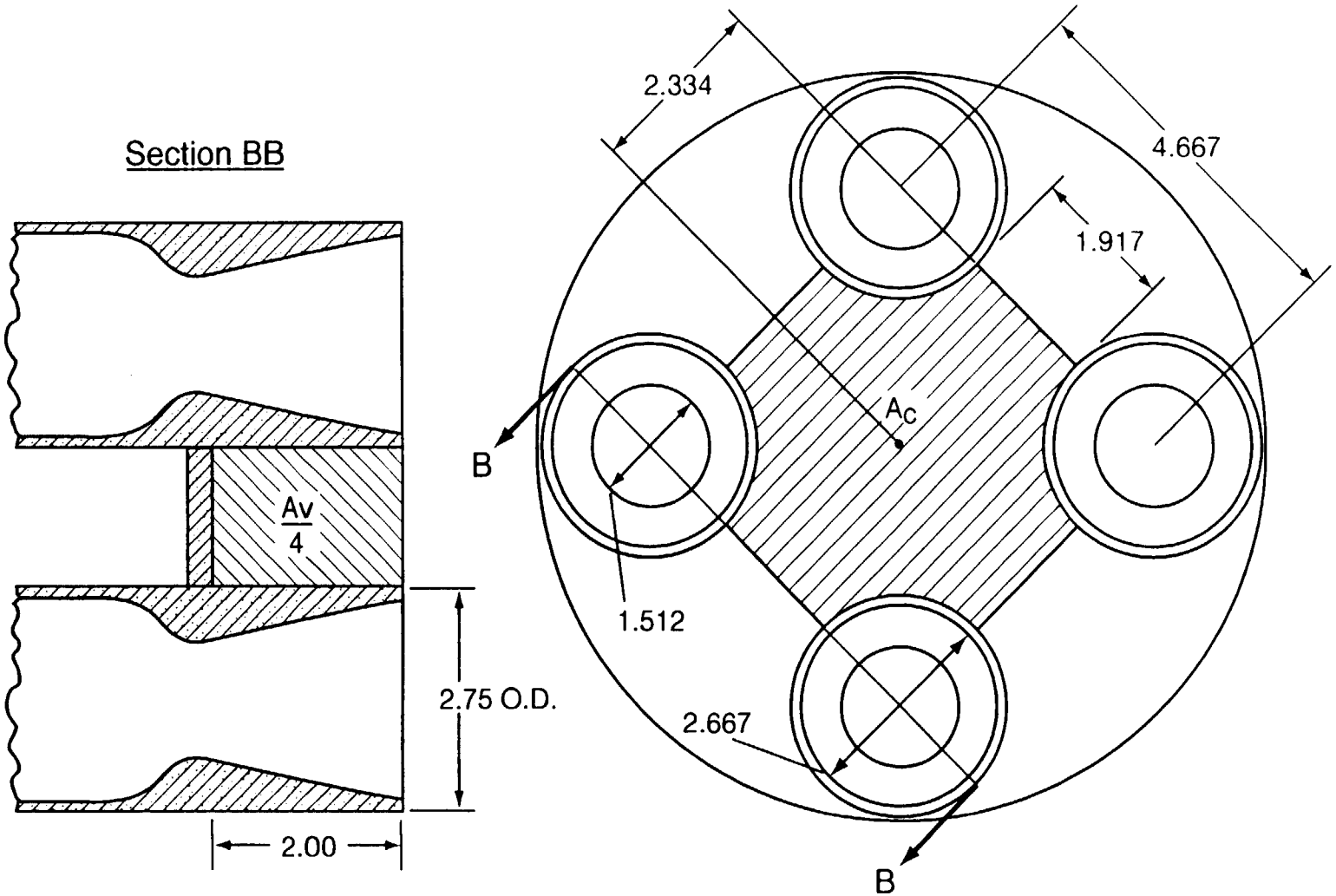

Fig. 2 Model configuration (dimensions in inches).

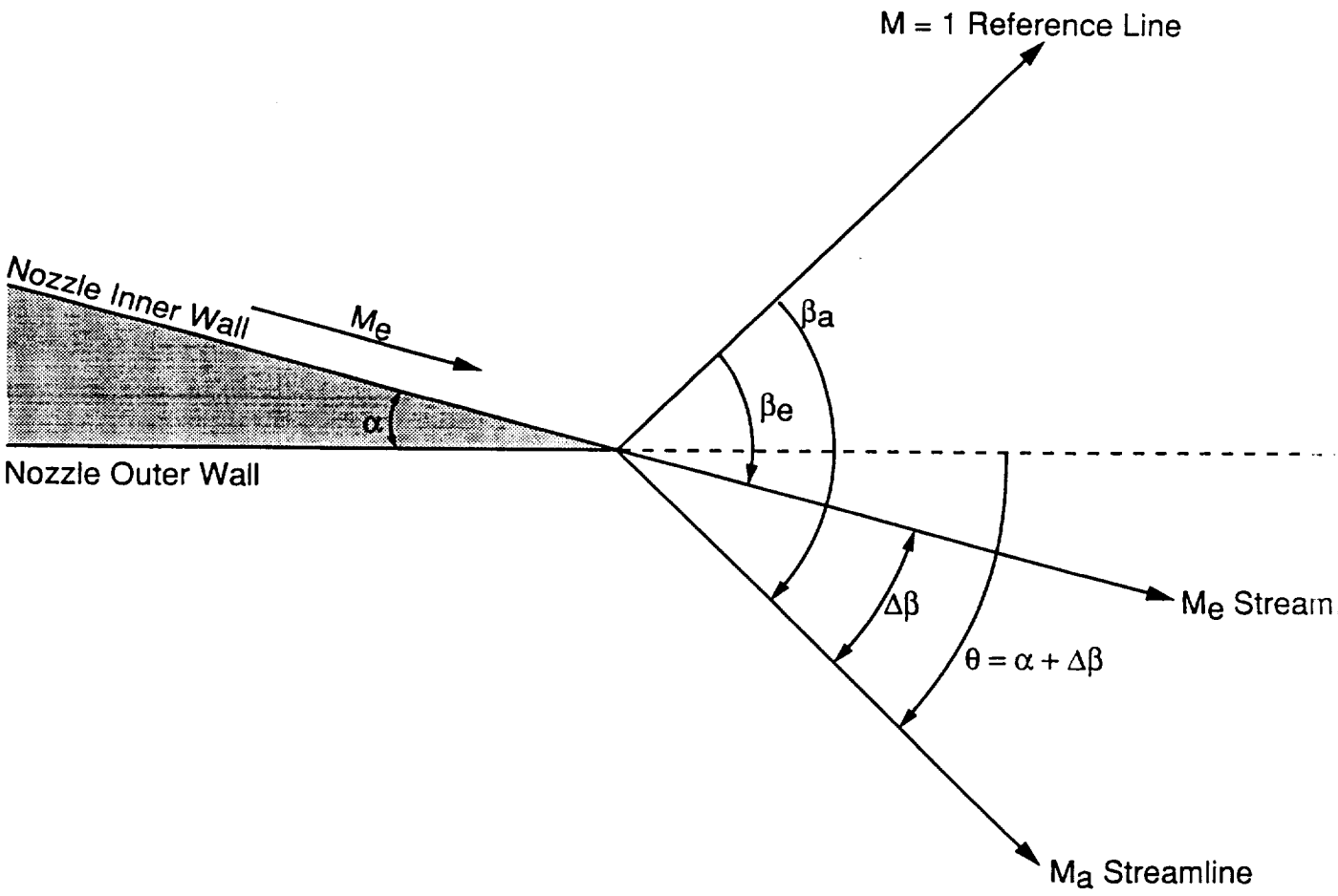

Fig. 3 Prandtl-Meyer expansion around the nozzle lip.

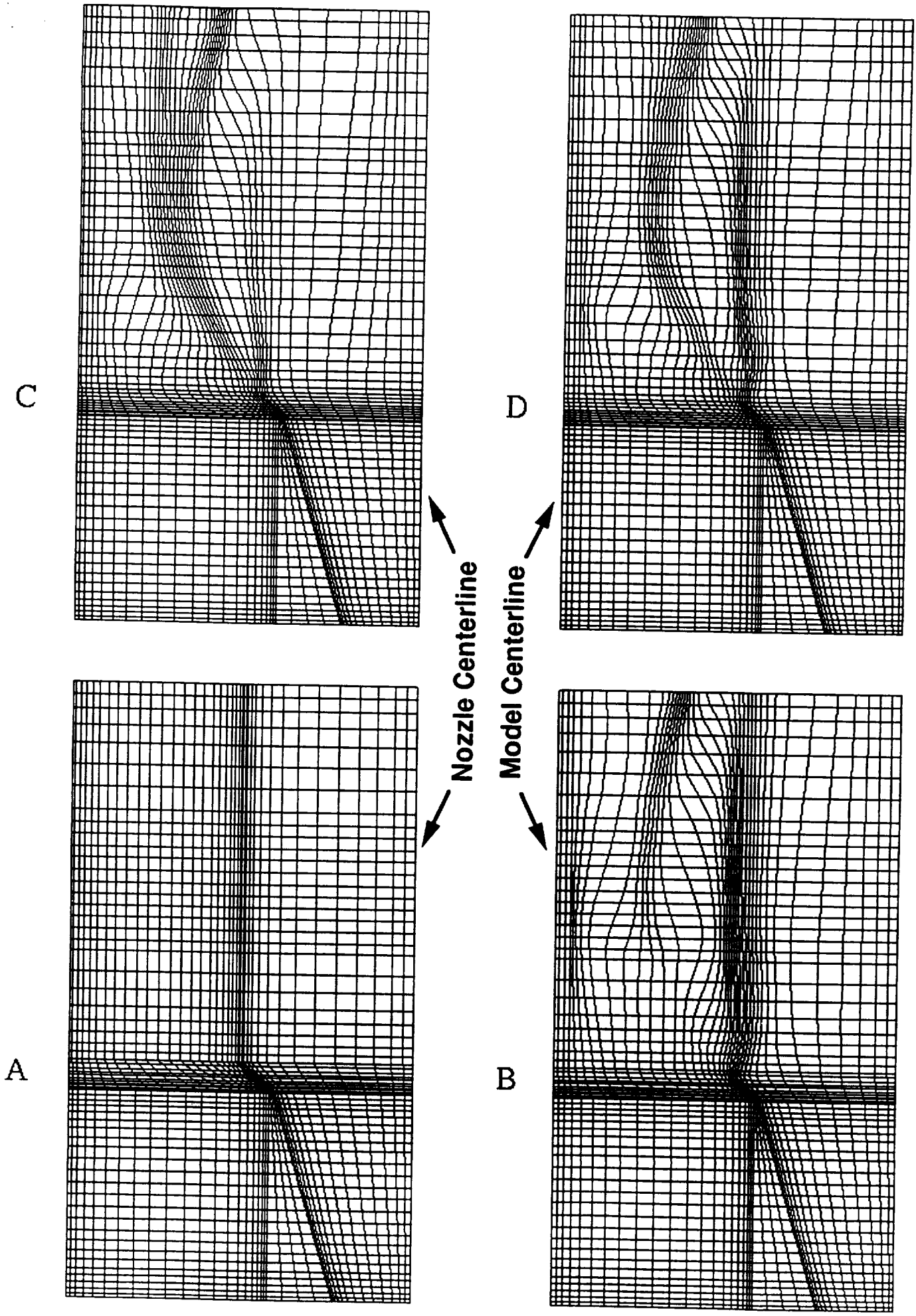

Fig. 4 Slices of four different computational grids.

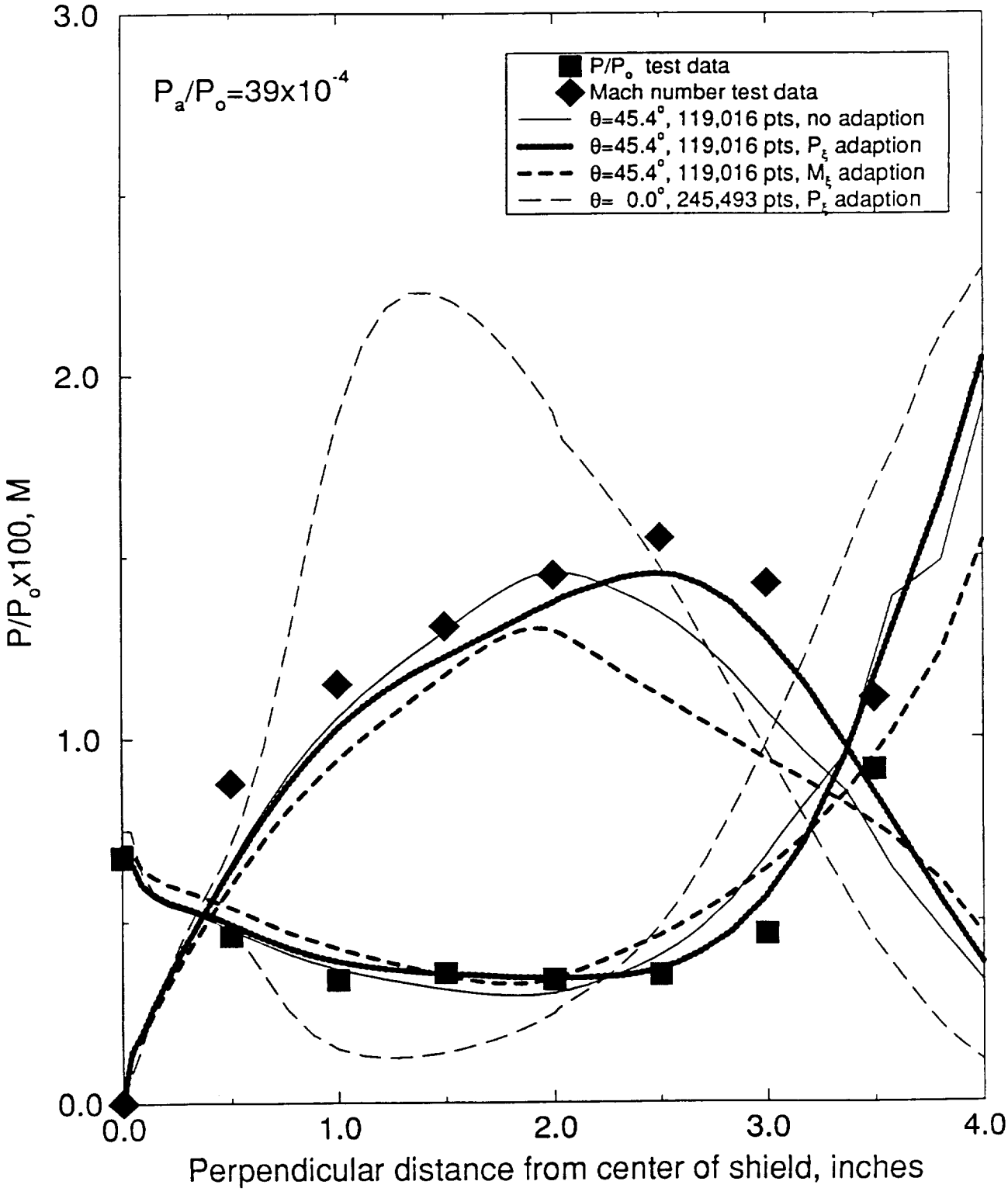

Fig. 5 Comparison of Mach number and static pressure variations along model centerline for $P_a/P_o = 39x10^{-4}$.

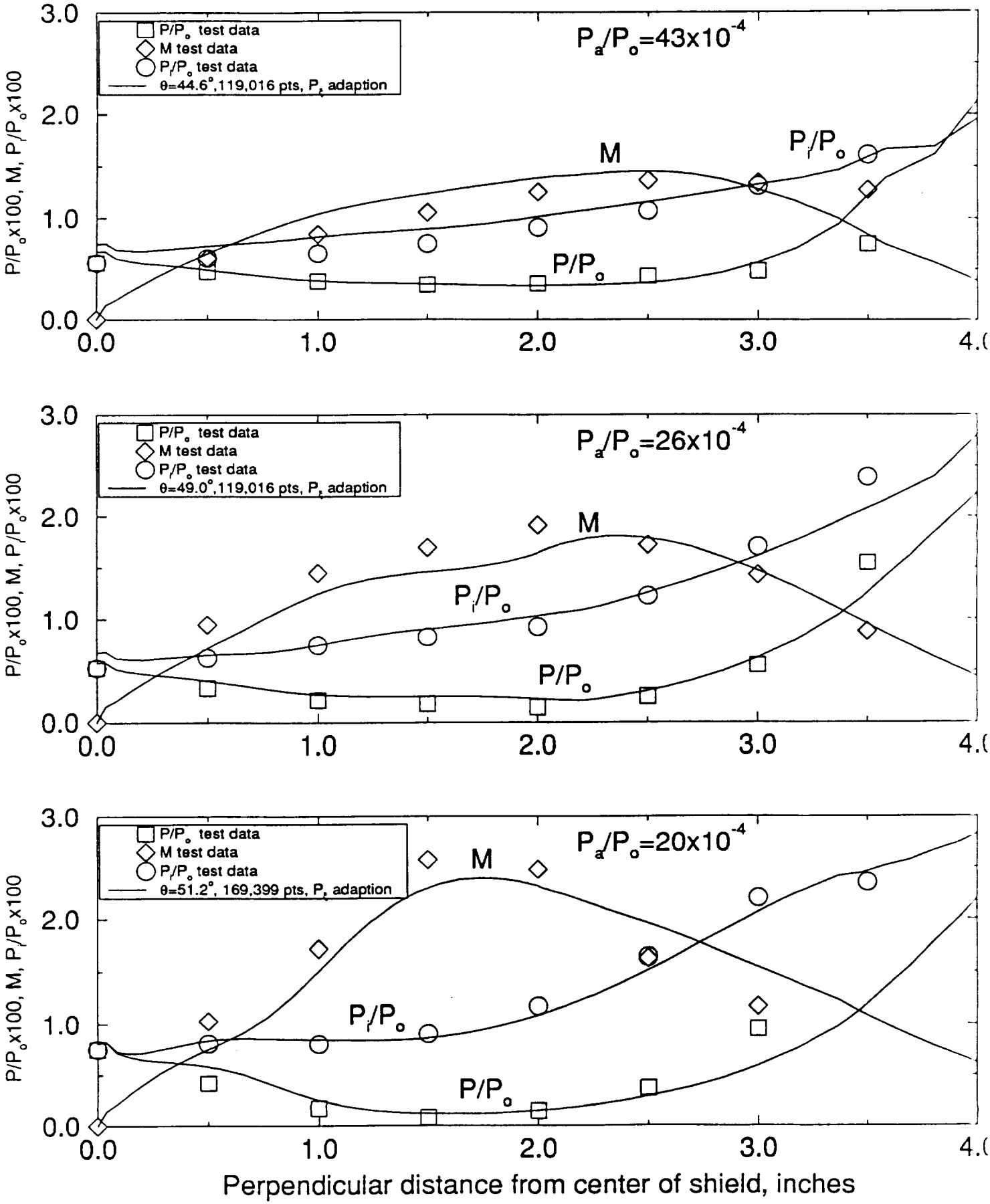

Fig. 6 Comparisons of static pressure, Mach number, and impact pressure variations along model centerline.

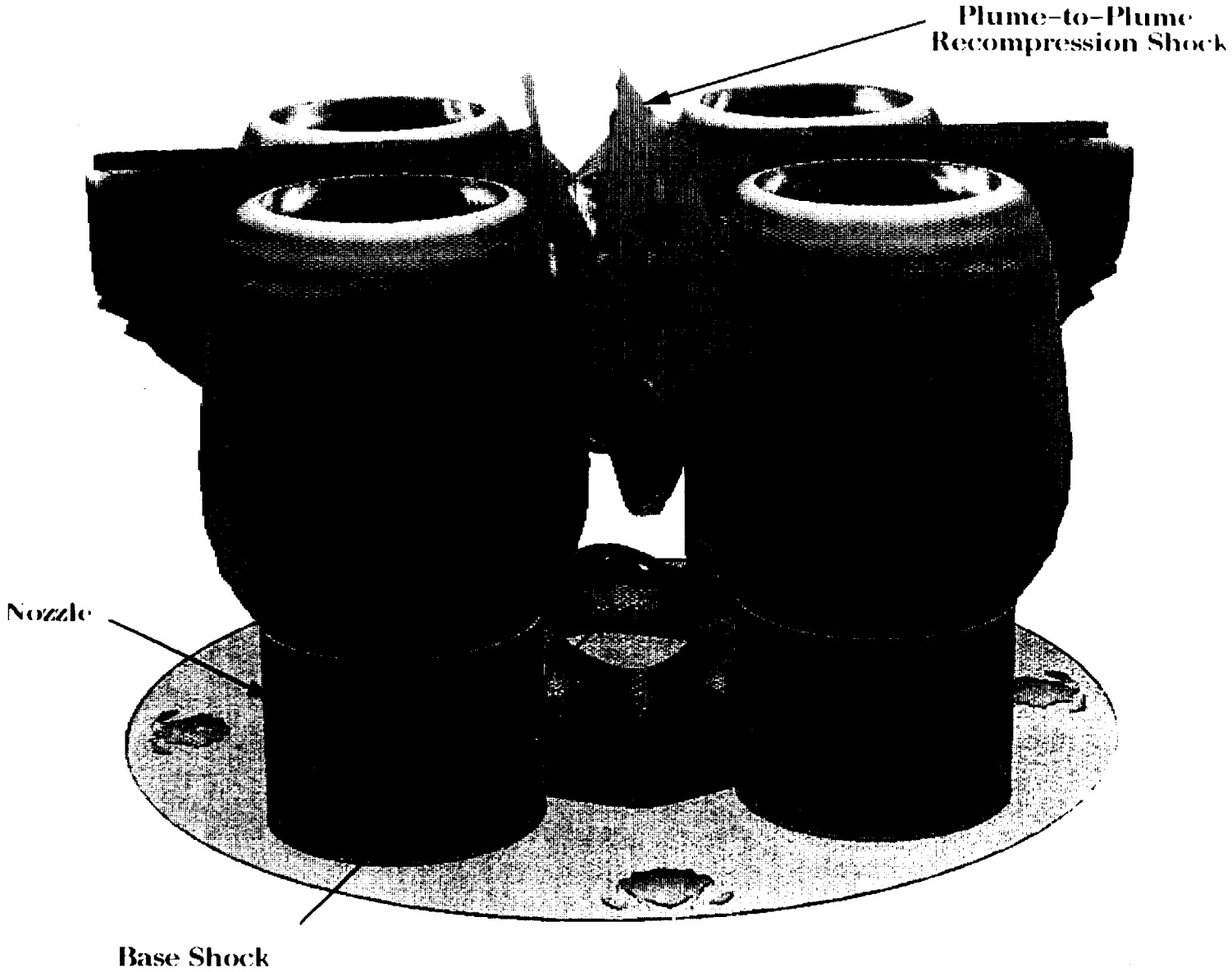

Fig. 7 Computed [illegible]

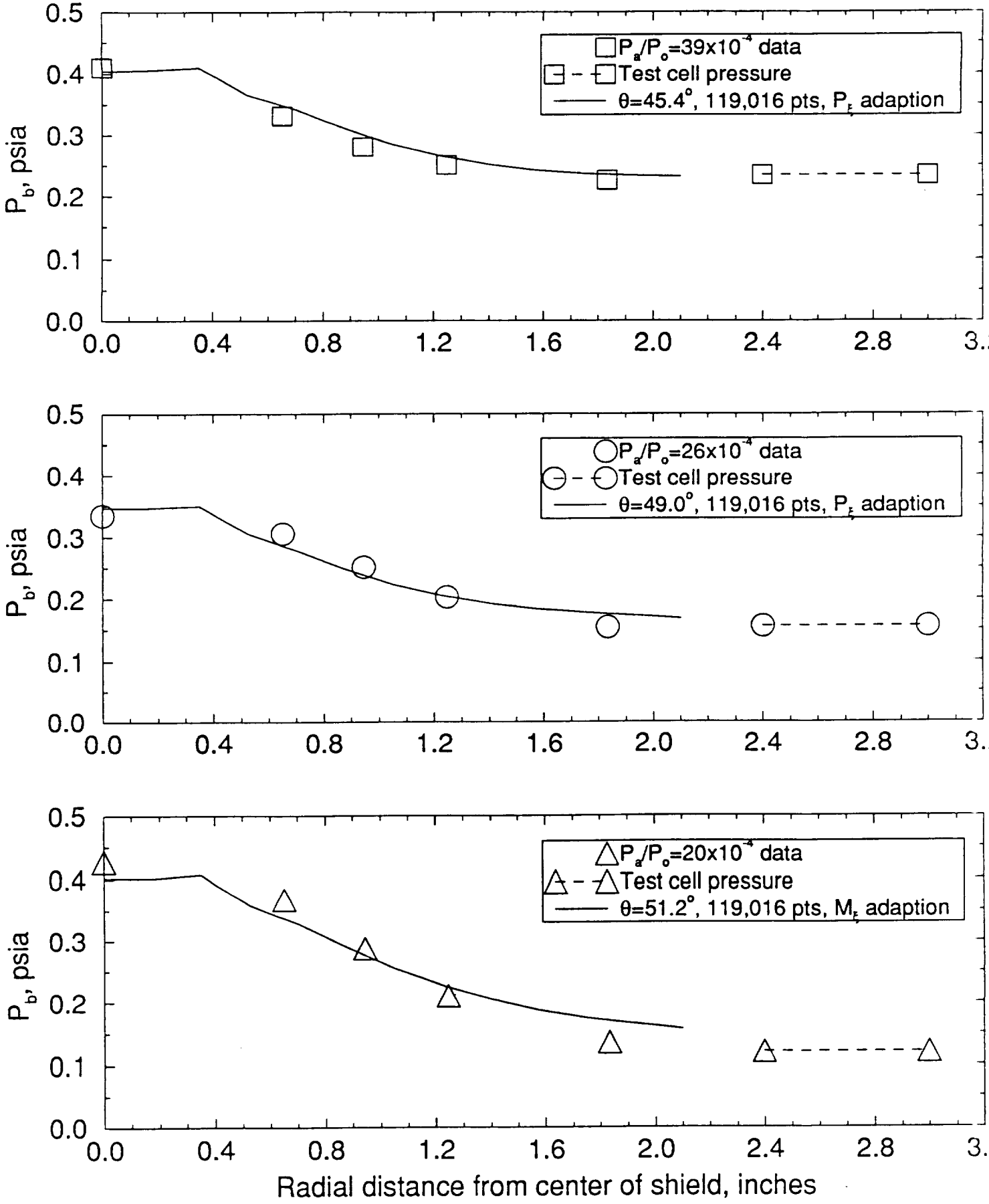

Fig. 8 Comparisons of radial base pressure distributions.

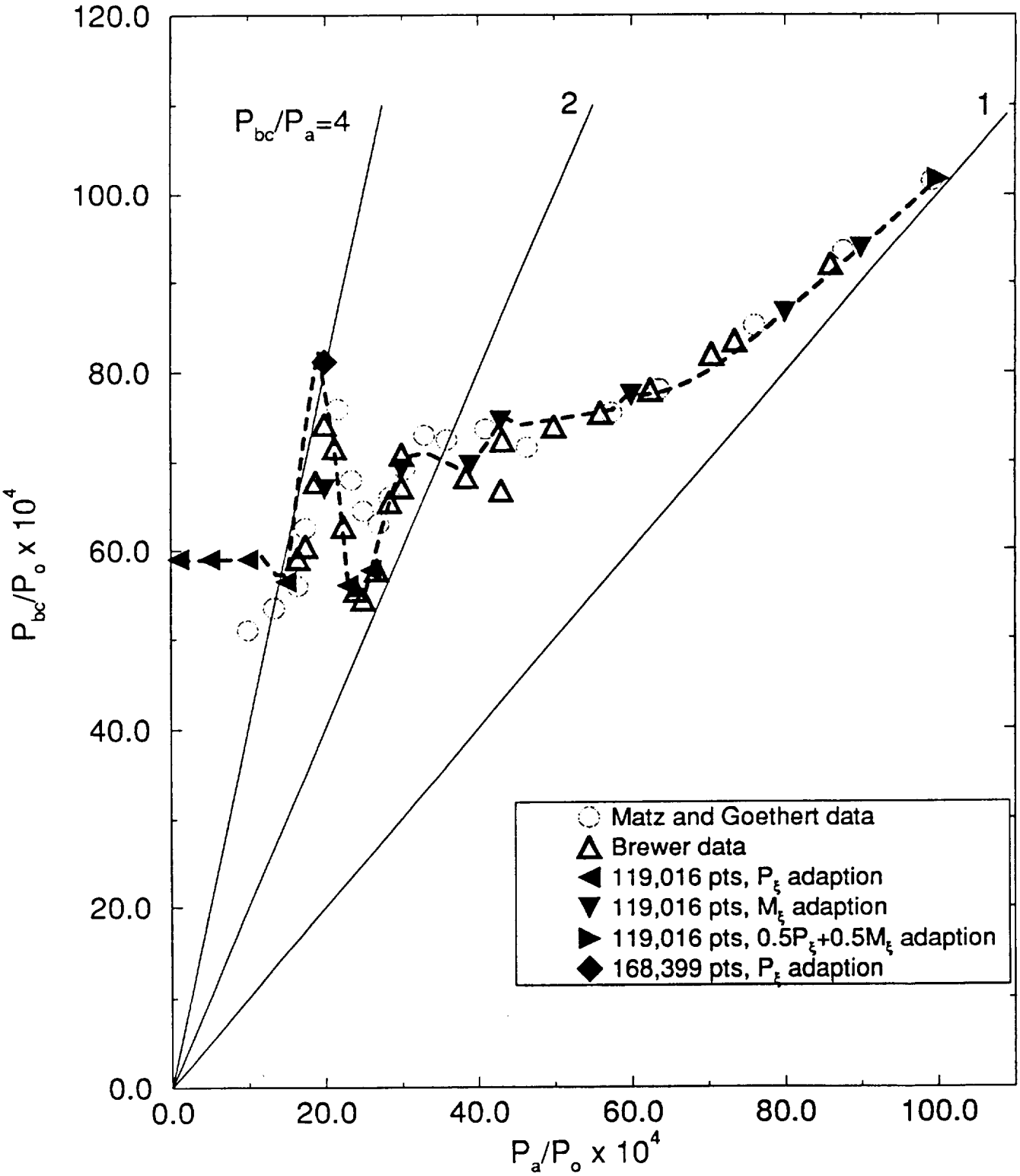

Fig. 9 Base Pressure Characteristic Curve.

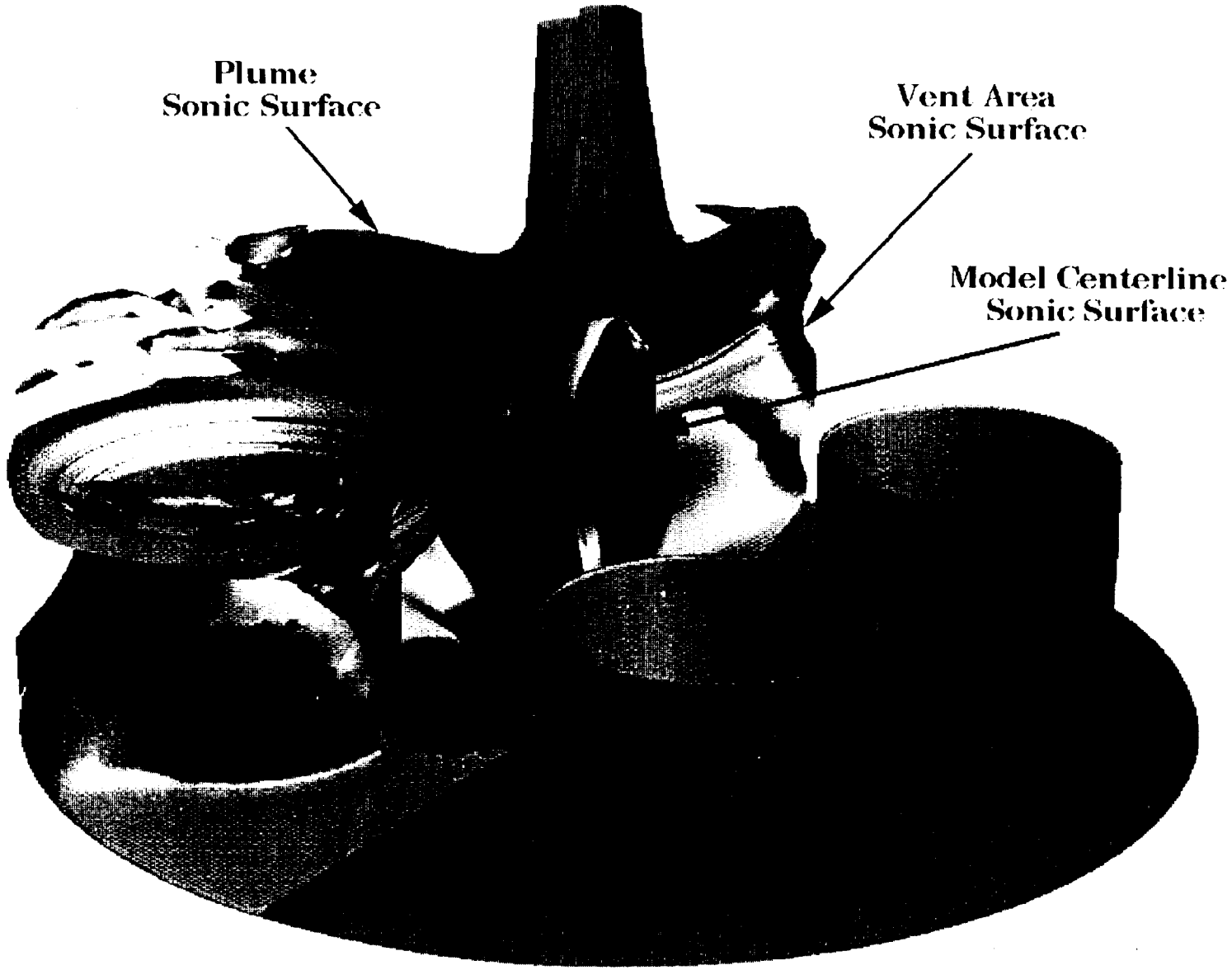
Plume
Sonic Surface
Vent Area
Sonic Surface
Model Centerline
Sonic Surface